Construction and Simulation of Low Resistivity Glass Resistive Plate Chamber (RPC) Detector

A thesis Submitted
in Partial Fulfilment of the Requirements
for the Degree of

MASTER OF SCIENCE

by

Soumik Chandra

to the

School of Physical Sciences

National Institute of Science Education and Research

Bhubaneswar

Date

DEDICATION

To my parents, teachers and my sister.

DECLARATION

I hereby declare that I am the sole author of this thesis in partial fulfillment of the requirements for a postgraduate degree from National Institute of Science Education and Research (NISER). I authorize NISER to lend this thesis to other institutions or individuals for the purpose of scholarly research.

Signature of the Student

Date:

The thesis work reported in the thesis entitled ..... was carried out under my supervision, in the school of ..... at NISER, Bhubaneswar, India.

Signature of the thesis supervisor

School:

Date:

ACKNOWLEDGEMENTS

I want to thank Prof Bedangadas Mohanty for allowing me to work in this project and for his guidance. I would also like to thank Dr Varchaswi K S Kashyap for his constant help and guidance throughout the project. I am thankful to Mr Subhash Rout for his help with the detector construction and Dr Abhik Jash for his help with the simulation. Finally, I wish to thank all the members of our lab, the faculties of the School of Physical Sciences and my friends in NISER for their support.

ABSTRACT

The upcoming collider experiments are aimed at a detailed observation of rare events. While the last few decades of effort has made it possible to collide protons at 13 TeV in the LHC, these new experiments are looking towards an increased luminosity. One of the challenges for a high luminosity collision experiment is having detectors with high rate capability and long lifetime. These are crucial since the detector should maintain optimum efficiency when exposed to high particle-flux. Resistive Plate Chamber (RPC) detectors are fast gaseous detectors designed to provide time-resolution of around 10 ns and also spatial resolution of a few cm^2, depending on the detector geometry. They are widely used as muon triggers in collider experiments. Low-resistive glass RPC detectors are expected to have higher rate capability than RPC made of ordinary glass. In this project, we have constructed RPC detectors using low resistive glass plates and ordinary glass plates and studying their properties as cosmic muon detectors. The gas mixture used in these experiments contains Freon (R134a) and iso-butane, with small amounts of sulphur fluoride. We also provide an estimate of the rate capability of this detector along with other properties like strip-multiplicity and efficiency curves for different thresholds. Also, a simulation of the detector using Garfield++ has been attempted.

Contents

List of Figures

List of Tables

Chapter 1

Introduction

The Standard Model of particle physics, laid down in the 1960s, explains the three of the four fundamental interactions in nature. The Higgs boson got discovered in the CMS and ATLAS experiments at the Large Hadron Collider, CERN in 2012. This discovery has almost completed the Standard Model. Despite its enormous success, it has a few short-comings. To address those problems, the scientific community is developing experiments that would provide more precision and more significant data.

Two major collider-based experiments are under construction to push the experimental boundary of particle physics. The Compressed Baryonic Matter (CBM) experiment is an upcoming experiment at the Facility for Antiproton and Ion Research (FAIR) in Darmstadt. The CBM detector is designed to measure the collective behavior of hadrons, together with rare diagnostic probes such as multi-strange hyperons, charmed particles and vector mesons decaying into lepton pairs with unprecedented precision and statistics. Most of these particles will be studied for the first time in the FAIR energy range. In order to achieve the required precision, the measurements will be performed at reaction rates up to 10 MHz.

The High-Luminosity LHC, which should be operational from the end of 2027, will allow physicists to study of known mechanisms in greater detail, such as the properties of the Higgs boson, and observe rare new phenomena that might reveal themselves. For example, the High-Luminosity LHC will produce at least 15 million Higgs bosons per year, compared to around three million from the LHC in 2017.

1.1 Gaseous Detectors

Gaseous detectors are a class of detectors equipped with a sensitive gaseous medium. The early designs of gaseous detectors resembles the Geiger-Muller detector. In these detectors, an incident charged particle leads to ionization inside the medium. A strong electric field is applied inside the medium which leads to further ionization. This phenomenon is called electron avalanche. The anode is also connected to a circuit and it collects the electrons producing a signal. This detection mechanism has been used extensively.

Resistive gaseous detectors are a different version, with a slightly different working principle. They also have a sensitive gaseous medium but, at least one of the electrodes have high resistivity, of the order of 10^8 Ωcm or above. Examples of such detectors are **Spark Counters** and **Resistive Plate Chambers**, the later is a modified version of the former. The detection mechanism is slightly different. Here, the electrons produced due to ionization are not directly collected to obtain a signal for an incident charged particle. Instead, conductive plates or strips are placed outside the detector. When an electron avalanche is created, the motion of the charges inside results in the change of electric flux in the surrounding region, causing induction of a current on the conductive plates or strips. This current is collected using an external circuit to obtain the signal.

1.2 RPC Detector: Overview

The design of a single-gap RPC detector is fairly simplistic. A schematic diagram of the cross-section is shown in Fig 1.1. It consists of a gas-gap enclosed with resistive plates and spacers. Usually glass or bakelite plates are used for constructing RPC detectors. Conductive layers are applied on the outer surfaces of the plates through

which a high potential difference is applied. A mixture of freon and iso-butane, with minute quantity of sulphur fluoride, flows in and out of the gas gap. The signal is obtained using readouts placed above and below the chamber. They are insulated from the plates using Mylar sheets.

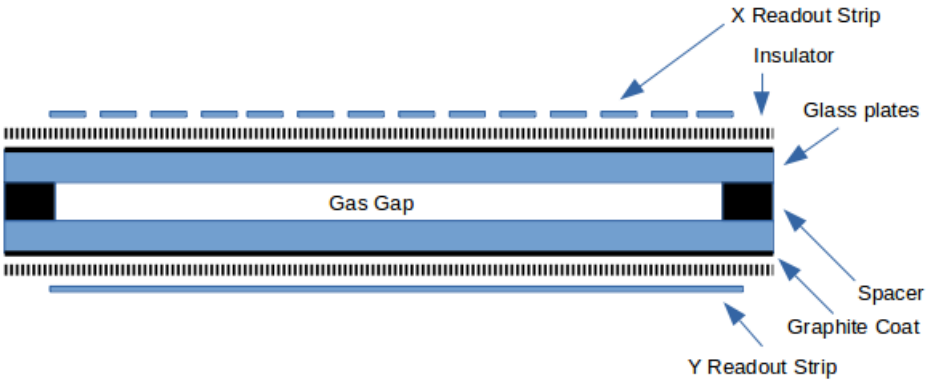

Figure 1.1: Schematic diagram of RPC cross-section

Features

The RPC detectors owe their effectiveness to these salient features:

- The RPCs provide a time resolution ∼10 ns and the response time to an incoming radiation is of the order of few nanoseconds. Hence, they can be used as trigger detectors as they provide almost full efficiency in optimum condition.
- The readout-strips are few centimeters wide. Using perpendicular strips below and above the RPC chamber, the x and y coordinates of the incident particle can be estimated. The spatial resolution is determined by the detector geometry.
- The electronics for collecting signals from an RPC detectors are simple and requires minimum processing, since they are based on induction of charge on external readout strips.

1.3 Motivation

Since high reaction rate or luminosity would require faster detection of particles, RPC detectors with high rate capability are necessary. The current rate capability of the RPCs used extensively in the CMS experiment at CERN is $\sim$ 1 kHz/cm^2. For experiments with high luminosity like the CBM experiment at FAIR, this is an attempt to develop an RPC detectors with a rate capability of 10 kHz/cm^2. Besides, exposure to high flux of incident particles lead to faster degradation of the detectors. For RPC detectors, the charge carriers in the resistive plates are dissipated. When exposed to high flux, these detectors will be rendered useless before the completion of an experiment. Hence, this project is also aimed at designing a detector with long lifetime.

Chapter 2

Low-resistive glass RPC detector

The RPC detector is constructed with low-resistive glass plates. Usually, detectors are designed for high gain, so that an amplified and clear signal is observed. But, in order to increase the rate-capability of this detector, low gain is preferable.

The operation of an RPC is based on the working principle of **spark counters** and are designed to overcome the disadvantages of constructing large-scale fast detectors. RPCs do compromise in the time resolution but nanosecond resolution make them effective for fast detection of radiation. This project is based on the construction, characterization and simulation of a glass RPC.

2.1 Components

The construction of the RPC requires the availability of the following materials:

- **Glass plates**, clean and smooth, with no apparent irregularities on the surfaces.
- **Conductive paint**, graphite for instance, and an apparatus to spray it with on the glass plates.
- **Spacers** to maintain the required uniform gap in between the glass plates and seal the gas gap.
- **Strong glue** to put the plates and spacers together and make the gas-gap leak proof so that it can sustain the gas mixture at higher pressure compared to the atmospheric pressure.

- **Copper strips** to provide potential to the graphite surfaces and to be used in read-out panels.
- **Mylar sheets**, which are plastic sheets made from PET, to provide insulation between the electrodes and the read-out panels.

2.1.1 The Resistive Plates

The resistive plates used in this project are made of ion-conducting glass. These plates differ from ordinary glass which has a bulk resistivity of the order of 10^{12} Ωcm.[1] These glass plates have a bulk resistivity of the order of 10^{10} Ωcm, and the are expected to provide higher rate-capability than ordinary glass plates. Another advantage of using low-resistive plates is the number of charge carriers inside the plates is more than ordinary glass, hence an RPC made of this will have a longer lifetime.

2.1.2 The Conductive Paint

The conductive paint is graphite paint. It is mixed with thinner and then sprayed on one side of each glass plate such that a conductive surface is available to provide potential difference to the glass plates. The painting needs to be uniform such that the entire surface has almost equal potential. To ensure that, the surface resistivity is measured in perpendicular directions at different parts of the plate surface.

2.2 The Gas Mixture

The gas mixture is the sensitive medium with which the radiation interacts and produces the signal. The radiation causes ionization along its track in the gas. The free electrons produced cause further ionization and the number of free electrons increase exponentially within a few nanoseconds, forming an electron avalanche. The

Figure 2.1: Resistive Plate with Graphite Coating

gas should have quenching property so that the discharge stays localized and sparks are avoided.

- Freon (1,1,1,2 - Tetrafluoroethane commonly known as R134a refrigerant) is used in the gas mixture and it is the primary constituent to create a discharge when radiation passes through the gas gap. The abundance of electrons in R134a and its property of forming electrons clusters are crucial in the formation of fast signals.

- The UV radiation produced due to interaction of the radiation with the gas are to be absorbed by the gas mixture, hence iso-butane is added to the mixture. The photons are absorbed by this gas and hence prevents further photo-ionization.

- To prevent high energy electrons from causing further discharges, electronega-

tive gas SF_6 is added to the mixture such that the electrons are absorbed and the exponential growth of the discharge is inhibited after a certain limit.

In this project, we have used three different gas mixtures with the following compositions:

- 95.2% Freon, 4.5% Iso-butane and 0.3% SF_6
- 94.5% Freon, 4.5% Iso-butane and 1% SF_6
- 93.5% Freon, 4.5% Iso-butane and 2% SF_6

2.3 The Read-Out Panels

There are two sets of read-out panels which are placed in perpendicular directions, along x and y axes. Each set is made of 10 separate strips of copper 2.8 cm wide and of the length of the RPC. The strips arranged parallel to the x axis are 0.2 cm apart and are used to get an estimate of the y coordinate of the point where the radiation passes through and vice versa. Thus, we get an estimate of the point of incidence, along with the time of incidence. There are conducting plates placed on the top of the readout panels 0.5 cm away.

In order to construct the read-out panel, copper strips of 0.1 mm thickness and 2.8 cm width are placed on a piece of cardboard and sealed using Mylar sheets. Each strip is separately connected to limo cables that are connected to multi-input fast amplifier and digitizer. This allows collection of signal from every strip simultaneously. For most of the experiments carried out, we have looked at signal obtained from one strip.

2.4 Detection of Radiation

In order to obtain insight into the process of detection, one can look at a solitary event of a cosmic muon passing through the detector. The processes occurring are discussed in succession.

- A muon with energy of around 2 GeV enter the gas gap. While passing through the gas, it causes a surge of electron in the presence of strong electric field of the order of 10^5 V/m. These primary ionization clusters amplify in charge by subsequent energy transfer through collisions inside the gas mixture and together make up a signal. For a gas gap of width of 2 mm, the time taken is around 10 ns. Since the avalanche growth is exponential, the cluster attains the maximum charge at the end of the process and electrons close to the cathode are responsible for maximum production of charge. It then causes a large and localized field drop before being deposited. This large field drop also leads to a damped growth of the signal once the cluster reaches a size of 10^6 to 10^7 electrons.

- To obtain time resolution in nanoseconds, the ionization cluster must be short-lived. It should not trigger ionization throughout the medium and cause secondary clusters. Any such cluster would prevent spatial localization of the radiation and also inhibit detection of further radiation until it dies out. To avoid such situation, both electrons and ionizing photons are to be absorbed by the gas mixture. Hence, SF_6 is used to quench the stray electrons at the end of avalanche and iso-butane is used to quench the ionizing UV photons.

- Strong electric field leads to exponential increase in the amount of charge produced and this is referred to as avalanche multiplication. It modifies the shape

of the signal obtained, the induced signal increases with time and attains its maximum before reducing to zero. Signal due to electron current attains the peak value with a sharp rise and drops abruptly while the ion signal shows gradual rise and fall.

2.4.1 Induction of Signal

The motion of these free electrons inside the gas gap induces a current on the conducting strip placed outside the gas gap. This can be exploited to obtain signal for charged particles passing through the RPC detector. The following factors are to be taken into account regarding the induction of charge in external conducting strip.

- **Charge of the avalanche:** The avalanche created due to the radiation must have enough charge to induce significant amount of charge on the external strips. Hence it is not an effective mode of collecting signals if the signals themselves are small.

- **Surface Resistance:** The surface resistance of the resistive electrodes need to be optimized. While a low surface resistance would allow faster transfer of charge deposited on the electrodes and helps boost the rate, high surface resistance increases the charge transparency of the resistive plate and allows better localization of the signal.

The process of signal induction is described by the Shockley-Ramo theorem. The instantaneous electric currents in a conductor induced by moving charges outside is given by

$$i(t) = \frac{E_W(w(t))v(x(t),t)}{V_W}q \tag{2.1}$$

where $v(t)$ is the instantaneous velocity of charge q, and E_W is the weighting field, with weighting potential V_W. This is the simplified form considering the velocity of

the charges is aligned to electric field. Generally, the quantity E_W/V_w is defined as the weighting field as well, which is the case here. The details of weighting field in this experiment is discussed in chapter 5.

2.5 Modes of Operation

The RPC can be operated in two different modes of operations namely the **streamer mode** and the **avalanche mode**. We have carried out our experiments in the avalanche mode for various advantages it provides in the current set of experiments.

- **Streamer Mode:** In this mode of operation, the potential difference maintained across the electrodes are high enough to allow secondary ionization, hence forming charge clusters of around 10^8 electrons. The intense electric field inside causes the gaseous medium to break down resulting in a continuous discharge which produces large signals. Thus, the signal obtained in streamer mode has higher amplitude. Since the relaxation time of the detector is less in this mode of operation it is not used when higher detection rate is essential or better time resolution is required.

- **Avalanche Mode:** In this mode of operation the electric field is kept just enough to allow the formation of electron cluster of the order of 10^6 to 10^7 and secondary discharges are prevented by introducing electron quenching gases like SF_6 in this case. As a result, the gaseous medium does not break down, rather relatively small surges of avalanches form when a radiation hits the detector. As a result, a sharper signal of lesser amplitude is obtained. This signal is still significant enough to be amplified and collected and serves the purpose of fast localized detection.

2.6 Achieving Avalanche Mode

The addition of electronegative gas like SF_6 determines the potential difference at which the avalanche mode of acquisition ends and the streamer mode begins. This is mainly due to the fact that SF_6 absorbs electrons and hinders the formation of a cluster beyond a given size for any potential difference. With this gas added, one can operate the detector at higher potentials without reaching the streamer mode of operation. Thus, as will be discussed later, we could operate the RPC at higher potential differences with increasing fraction of SF_6 into the mixture.

Chapter 3

Construction, Assembly and Signal Processing

The construction of the RPC detector has been accomplished in the Detector Lab RL-202, NISER. All the components and required equipment were made available by the efforts of the laboratory.

3.1 Components

The RPC detector is constructed and assembled with the following materials:

- **Glass plates**, clean and smooth, with no apparent irregularities on the surfaces.
- **Conductive paint**, graphite paint for instance, and an apparatus to spray it with on the glass plates.
- **Spacers** to maintain the required uniform gap in between the glass plates.
- **Strong glue** to put the plates and spacers together and make the apparatus leak proof so as to sustain pressure higher than atmospheric pressure inside the gas gap.
- **Copper strips** to provide potential to the graphite surfaces and to be used in read-out panels.
- **Mylar sheets**, which are plastic sheets made from PET, to provide insulation between the electrodes and the read-out panels.

3.2 The Resistive Plates

The resistive plates used in this project are ion-conducting glass. These plates differ from ordinary glass which has a bulk resistivity of the order of 10^{12} Ωcm. The glass plates used have a bulk resistivity of the order of 10^{10} Ωcm, and the experiments will let us see if this can help us achieve higher detection rate and better time resolution.

3.2.1 The Conductive Paint

The conductive paint is graphite paint developed for INO by Nerolac Kansai. It is mixed with thinner and then sprayed on one side of each glass plate such that a conductive surface is available to provide potential difference to the glass plates. The coating needs to be uniform such that the entire surface has almost equal potential. To ensure that, the surface resistivity is measured in perpendicular directions at different parts of the surface.

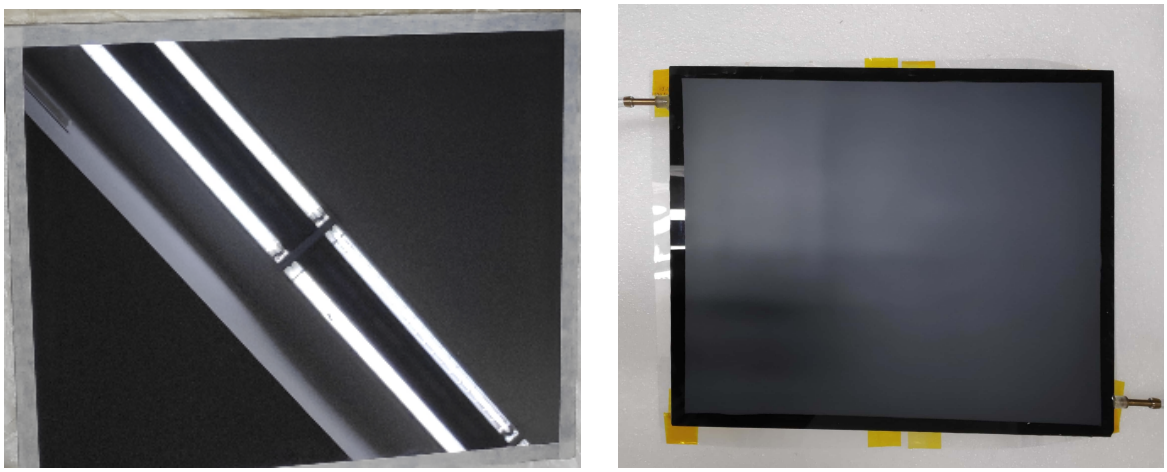

(a) (b)

Figure 3.1: (a) Low resistive glass plate before the application of conductive paint. (b) Resistive plate with graphite coating.

Graphite paint is ideal for this case since it can be applied in very fine layers. The graphite paint is mixed with paint-thinner so that it can be easily sprayed on the glass

surface. It is then sprayed on the surface using a spray paint apparatus. Special care is to be taken to make the painting uniform so that the surface resistivity remains constant throughout the surface. Achieving such precision manually is somewhat far fetched, so the surface resistivity varies throughout the surface and we take the mean of the values at different regions.

The surface resistivity plots for electrodes of an RPC are shown in Fig. 3.2. The mean resistivities of plates in are around 0.5 MΩ/□.

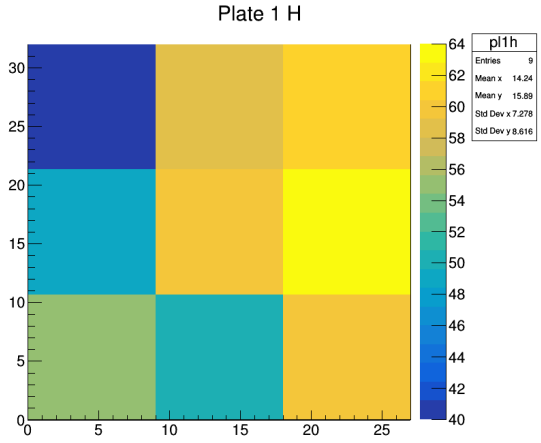

(a) Surface resistivity of Plate 1 in horizontal direction.

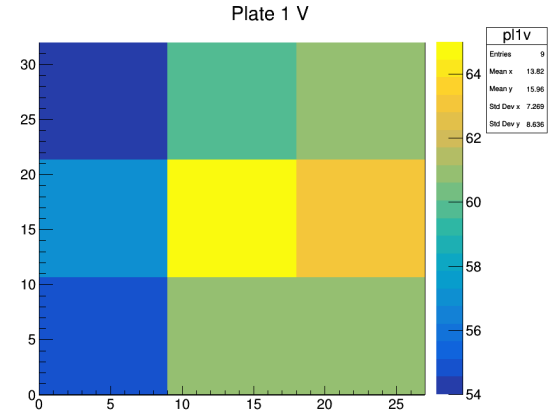

(b) Surface resistivity of Plate 1 in vertical direction.

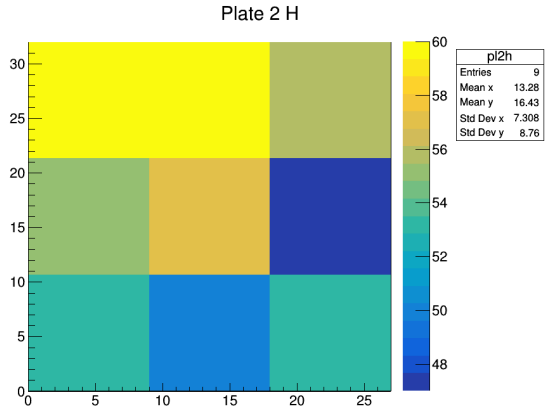

(c) Surface resistivity of Plate 2 in horizontal direction.

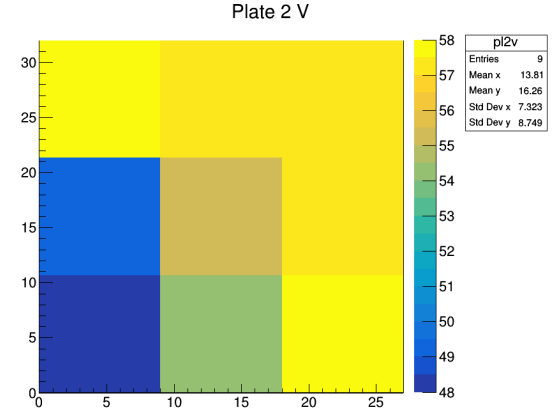

(d) Surface resistivity of Plate 2 in vertical direction.

Figure 3.2: Surface resistivities of the glass plates after graphite paint is applied.

3.3 The Read-Out Panels

There are two sets of read-out panels which are placed in perpendicular directions, along x and y axes. Each set is made of 10 separate strips of copper 2.8 cm wide and of the length of the RPC. The strips arranged parallel to the X axis 0.2 cm apart and are used to get an estimate of the Y coordinate of the point where the radiation passes through and vice versa. Thus, we get estimate of the point of incidence, along with the time of incidence.

In order to construct the read-out panel copper strips of 0.1 mm thickness and 2.8 cm width are placed on a piece of cardboard and sealed using Mylar sheets. Each strip is separately connected to LEMO cables that are connected to multi-input fast amplifier and digitizer. This allows collection of signal from every strip simultaneously. For most of the experiments carried out, we have looked at signal obtained from one strip.

3.4 Region of avalanche mode operation

The addition of electronegative gas like SF_6 modifies the potential difference at which the avalanche mode of operation ends and the streamer mode begins because SF_6 absorbs stray electrons and hinders the formation of a cluster beyond a limit for any given potential difference. With this gas added, one can operate the detector at higher potentials without reaching the streamer mode. Thus, as will be discussed later, we could operate the RPC at higher potential differences with increasing fraction of SF_6 into the mixture. However, even under avalanche mode operation, occasional streamers do occur. The addition of SF_6 helps to reduce the occasional streamers or the so called **Streamer fraction**.

The construction of the RPC was the foremost aim of the project. Right now, we

have two functional RPC detectors in the laboratory and we have finished the process of characterization for one of these. The next few sections discuss the details of the construction and assembling the RPC detector for muon detection.

3.5 Glass as electrode

The RPC detectors are constructed of glass with lower bulk resistivity as mentioned before. The benefits of using this low resistive glass are as follows:

- Glass surfaces are inherently more smooth compared to surfaces of polymer sheets that are generally used to construct RPC detectors. As a result, the noise rate decreases since regular surfaces do not cause abrupt discharges. These discharges can be mistaken as signals and are caused mainly by sharp or point-like irregularities on the inner surface of the resistive plates.

- Having lower bulk resistivity helps maintaining the required electric field inside the gas gap even without having a low surface resistivity. Hence, it would allow us to obtain better localization of the signal since even a thin layer of graphite would allow uniform distribution of the electric field. The bulk resistivity of the plate used is 1.5×10^{10} Ωcm and has a dielectric constant between 7.5 and 9.5, and the surface roughness is less than 10 nm[1].

- An incident charged particle leads to the formation of electron avalanches inside the gas gap. Under the influence of the strong electric field, the avalanche is finally deposited in the anode. This causes an instanteneous drop in the potential difference between the electrodes. The rate capability of an RPC is the achieved rate per unit potential drop across the electrodes. The mean charge deposited inside the gas gap can be used to calculate the rate capability of the

detector using the following relation[2]:

$$\text{Rate capability} = \frac{V}{\rho \langle Q \rangle t} \tag{3.1}$$

where, ρ is the bulk resistivity of the electrodes, t is the total thickness of the two electrodes, $\langle Q \rangle$ is the average charge deposited inside the gas gap and V is the potential drop across the electrodes due to a signal. The ratio of the mean charge deposited inside the gas gap $\langle Q \rangle$ to the charge induced on the strip due to prompt charge $\langle q \rangle$ is generally ~ 25. The rate capability of the RPC is inversely proportional to the bulk resistivity of the resistive plate, hence using low resistive glass is expected to enhance the rate capability by orders of magnitude.

3.6 Putting the RPC together

Once the graphite coating shows almost uniform resistivity with mean resistivity close to the desired value, the plates need to be put together with spacers in between to create the required gas gap. During this process, the inlet and outlet of gas mixture are also put in place. The procedure followed is mentioned below.

- The clear side of the glass plates are cleaned using alcohol and tissues to remove dusts and smudges.
- The spacers are cut into 4 pieces of proper length and placed on the edges of the glass plate along with the inlet and outlet of gas mixture to ensure they fit properly enclosing the gas gap.
- Araldite has been used as the strong glue. It is prepared by mixing a latex with a hardener, which becomes a strong glue only when mixed together. Equal

amounts of both are mixed thoroughly to prepare the glue. Once mixed, it can be used for around 30 minutes before it starts hardening.

- A button spacer is placed at the center of one plate with glue and more is added on the top. The side spacers are glued to one plate maintaining equal gaps on all sides. Then the other plate is put on the top after glue is applied to all sides of the spacers. The gas inlet and outlets are placed in diagonally opposite ends.

3.7 Testing for leak

In order to make sure that the gas mixture stays inside the gas gap of the RPC, one should find and plug all leaks. While utmost care is taken to make sure no such gaps exits during assembling the RPC, one still needs to test for leaks. The apparatus for performing a leak test is shown below. A pressurized argon cylinder is used to create a pressure of about 20 - 30 mm water above atmospheric pressure inside the RPC. The RPC is then connected to a manometer and the difference in water level is monitored for around 6 hours.

Initially, we found a small leak rate in both the RPCs but they were plugged by regluing and finally, the drop in pressure was less than a millimeter in 6 hours, which is a negligibly small leak rate. Hence for our purpose of operation, the RPCs are effectively leak-proof.

3.8 Assembling the detector

The gas inlet of the RPC is connected to the outlet of the gas mixing apparatus. It is then placed between two readout panel and two Mylar sheets for signal collection and insulation respectively. The cross-section of the combined structure is shown in Fig. 1.1. We have placed scintillators above and below the detector to be used as

Figure 3.3: Apparatus for leak test

external trigger as shown in Fig. 3.4.

One copper strip is attached to each graphite coating to apply potential to the glass plates and they are soldered to wires. These are then connected to a programmable high voltage source CAEN Mod. N1470 which are controlled using CAEN software. The details of the electronics used are described in the next chapter.

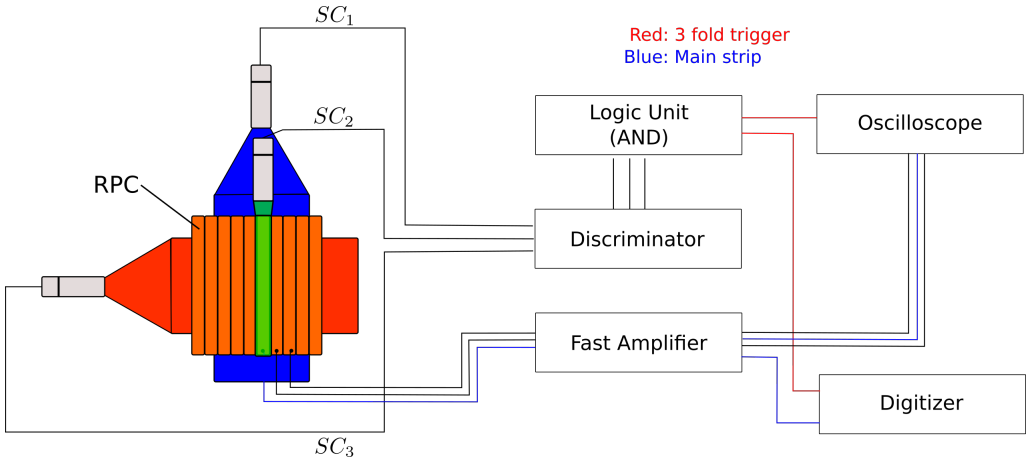

Figure 3.4: Schematic Diagram of RPC

Figure 3.5: The Detector Setup

3.9 Flushing the RPC and spark test

With the detector assembled, the gas mixture is made to pass through the RPC gas gap for at least a day or two to remove air and any small dust particle trapped inside it. Once the RPC is conditioned, the potential is then applied gradually to the electrodes and the current is observed.

While the current will be large even at lower potential difference in the beginning, as the gas flushes out the air and dusts, the current keeps decreasing as there are fewer sparks inside the gas gap. This would conclude the spark test as there are no sparks or large surges of current inside the gas gap, or the medium does not break down to become conductive. This is crucial to maintain the detector in avalanche mode.

Concluding tests

High voltages are required to obtain signals from the RPC even for 0.3% SF_6 gas in the mixture. The minimum potential needed is 9.8 kV. In order to keep the sparks at minimum, the **Relative Humidity** (R.H.) of the room needs to be below 60%. We have used 3 dehumidifiers and an air conditioner to maintain the R.H at $\sim 50\%$ in order to achieve working conditions.

3.10 Data acquisition and processing

The electronics of the detection process is mainly composed of NIM (Nuclear Instrumentation Module) and VME (Versa Module Eurocard) modules, LEMO cables and connectors. All the modules used in the process are described in chapter and their function in the detection process. The effective circuit diagram for the detector is described.

3.11 DAQ: Components and Functionality

The data acquisition system used in these experiments are CAEN modules. The following enlists all the modules used for detection:

- N1470 4 Ch Reversible 8 kV/3 mA (8W) NIM HV Power Supply Module (USB)
- N840 8 Channel Leading Edge Discriminator
- N979 16 Channel Fast Amplifier
- N405 Triple 4-Fold Logic Unit/Majority with VETO
- N1145 Quad Scaler And Preset Counter / Timer
- V1730 16/8 Channel 14 bit 500 MS/s Digitizer

3.11.1 N1470 (Power Supply)

The CAEN N1470 is used as the power supply for applying potential across the electrodes as well as the Photo-multiplier Tubes (PMTs) connected to the scintillator detector. Each channel can provide a ±8kV maximum voltage, a 3 mA max current and a 9 W max power (8 W max power when output voltage is larger than ±3 kV). The output polarity can be independently selected for each channel. The power supply is reversible which allows inverting the applied potential in the detector without the need of physically turning over the detector.

3.11.2 N840 (Discriminator)

The CAEN Mod. N840 is an 8 Channel Leading Edge Discriminator contained in 1-unit NIM module. The module accepts 8 negative inputs and produces 2×8 NIM outputs and 8 NIM outputs (negated) on front panel LEMO 00 connectors. The pulse forming stage of the discriminator produces an output pulse whose width is adjustable in a range from 5 ns to 40 ns. The discriminator thresholds can be selected individually in a range from -1 mV to -255 mV (in steps of 1 mV), via an 8-bit DAC. The minimum detectable signal is -5 mV.

3.11.3 N979 (Amplifier)

The Mod. N979 is a 16 channel fast rise time amplifier contained in a 1-unit NIM module; each channel features a fixed voltage gain of 10. Channels are bipolar, non-inverting. Channels can be cascaded in order to obtain larger gain values. Each channel is provided with three LEMO 00 connectors, one for the input and two bridged for the output. The board features a ±2 V output dynamics. 16 screw-trimmers (one per channel) allow the offset calibration which operates over a ±30 mV range.

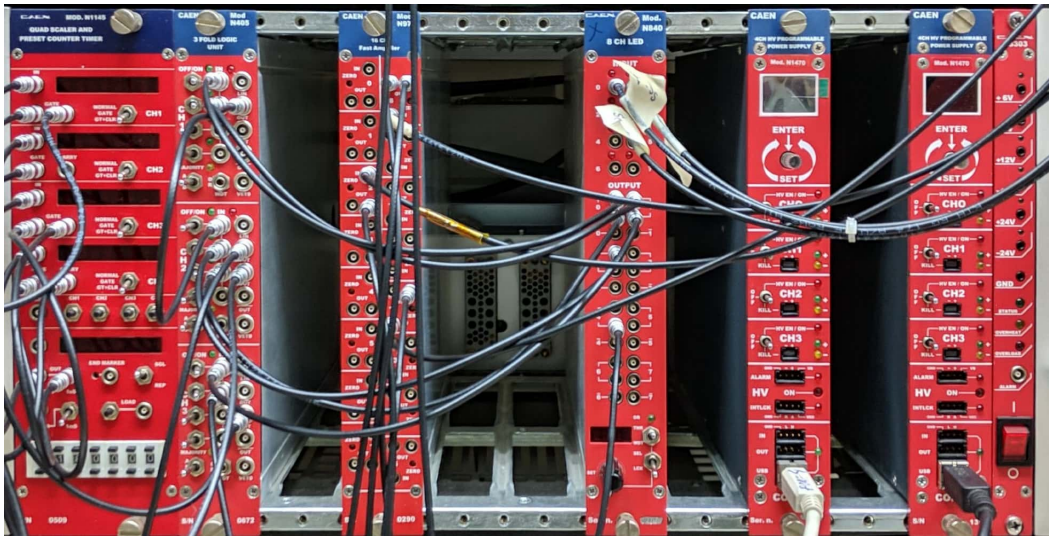

Figure 3.6: The Electronics used for Detection

3.11.4 N405 (Logic Unit)

The Mod. N405 is a one unit wide NIM module housing three independent sections that can be used either as logic unit or majority. The two modes are selectable via internal DIP switches. It is used mainly to perform coincidence experiments or in order to perform localization for particular strips. This is used to take coincidence of signals from three scintillators which is then used as trigger.

3.11.5 V1730 (Digitizer)

The V1730 is a CAEN Waveform Digitizer able to perform basic waveform recording and run online advanced algorithms (DPP) for digital pulse processing: charge integration and pulse shape discrimination with constant fraction timing, pulse height analysis, zero-length encoding, and dynamic acquisition window. A wide selection of DPP algorithms is supported by this digitizer.

3.12 Signal Processing

There are two sets of independent sets of electronics at work here, one for the RPC and one for the read-out panels. The former one is simply applying potential against a high resistance component which allows a constant current in the absence of radiation. The potential is of the order of 10 kV while the current is of the order of few μA.

The latter is the electronics of the read-out strips. This functions based on the principle of charge induction on conductors. Since the read-out strips are connected to a digitizer through a series of electronics, we can collect these induced charges. Since the charge is induced in a time interval of few nanoseconds, the output in the digitizer is a pulse of width of few nanoseconds. The pulse is integrated over the entire time interval to obtain the total charge induced on the strip.

The signal processing is constituted of the following processes:

1. The signal from a scintillator detector is passed through the CAEN Mod. N840 leading edge discriminator and amplifier.

2. This signal is then used as external trigger for the V1730 module, the signal from the readout strip is collected only when the scintillator gets a signal.

3. The readout strip is connected to the discriminator in order to remove low amplitude noise from the signal.

4. The output from N840 goes into the CAEN Mod. N979 fast amplifier where the signal is multiplied by a factor of 10.

5. The output from N840 is directly fed into the CAEN V1730 digitizer.

3.13 Other modes of data acquisition

There are other modes of data acquisition than collecting signals from a single strip. One experiment involves measuring the multiplicity of the strips and performing localization studies of the radiation using multiple strips.

3.13.1 N1145 (Counter)

The Mod. N1145 is a double unit NIM module that includes four independent 8-digit counters each with their own display and can accept up to 250-MHz input rates. This can be used to keep count of the number of muons passing through the RPC which can be used to calculate the muon flux.

3.13.2 Setup for Multiplicity

For calculating multiplicity, we need to collect signals from more than one strip of the readout. In our experiment, we have chosen to take data from 3 strips, one directly below the scintillator paddle, and two strips adjacent to it. The strip directly below is marked as strip 1, the one adjacent to strip 1 is marked strip 2 and the one adjacent to it is strip 3. Thus strip 2 lies between strip 1 and 3. In terms of distance from the paddle, strip 1 is closest followed by strip 2 and 3.

The detection process can be carried out in 2 ways:

- Online method, where the signals from three strips are passed through AND logic gate so that coincidences are recorded.
- Offline method, where the data is saved in list mode with time stamps that can be compared later to find coincidences.

To perform the strip multiplicity experiment, the offline method has been used.

Chapter 4

Detection of cosmic muons

The detector is designed for high luminosity experiments like CBM experiment or HL-LHC. Yet, due to unavailability of high flux muon source at our lab, we chose cosmic muons to be the source for our experiments. This causes an inherent inconvenience, the efficiency versus flux cannot be plotted. Instead, an indirect approach is taken to estimate the rate capability of the detector.

4.1 Cosmic muons

Cosmic muons are a result of the shower of Cosmic rays on the Earth's atmosphere, which are radiations arriving from outside the Solar System. Though Cosmic rays contain a wide range of particles and a significant number of protons, after colliding with the upper atmosphere, only a few particles get to reach the surface of the Earth. Since electrons get easily absorbed by the atmospheric gases along with X-rays, the only dominant radiation reaching the surface is muons. Most of the cosmic muons are produced through the following mechanism:

$$\pi^- \rightarrow \mu^- + \bar{\nu}_\mu$$

Muon belongs to the family of leptons, particularly in the second generation. It has a mass of around 105 MeV and decays into electron, neutrino and anti-neutrino through weak interaction with a mean lifetime of 2.2 μs.

$$\mu^- \rightarrow e^- + \bar{\nu}_e + \nu_\mu$$

Since some of the muons have high enough energy ($\sim$ 1 GeV) they travel at velocities close to c and survive long enough to reach the surface due to time dilation. These muons are detected using the RPC. Since most of the muons are incident normally on the surface of the Earth, we place the detector on a horizontal plane to increase the muon flux through the chamber.

4.2 Setting Trigger

The experiments are carried out by using scintillator detector as external trigger. These detectors are available in different sizes. The ones used in the experiments cover the different surface areas. One of them cover almost the same surface area as one strip. Since the trigger is taken from the AND output of the logic gate with inputs from 3 scintillators, every trigger is due to a muon passing through the RPC detector just below the strip. The arrangement of the scintillation detectors is shown in figure 3.4. A brief discussion on scintillator detector follows:

Scintillator Detector

A scintillator detector is composed of two parts, namely the **Scintillator** and the **Photo-multiplier Tube (PMT)**. The scintillator used here is made of plastic, which is mainly composed of hydrocarbons. When muons pass through the scintillator, it deposits part of its energy in the medium which is emitted by the medium as a photon. The photon is channeled to cause a photo-emission of electron and the number of electrons emitted is proportional to the energy of the photon.

Each electron passes through the PMT and multiplies in number and energy by application of high voltage through multiple electrodes and finally an amplified signal is obtained at the end. The output from the PMT is passed through the fast amplifier and discriminator into the external trigger port of the digitizer.

4.3 Obtaining Signal

Relative humidity (R.H.) and ambient temperate are the two important factors that affect the process of cosmic muon detection in this experiment. The relative humidity is defined as the ratio of the actual vapour density to the saturation vapour density. At right conditions with R.H. less than 60% and temperature 24^0C, we obtained the first signal in an oscilloscope along with the trigger. Due to the electronic delay induced in signal processing while generating the trigger (square wave pulse), it precedes the trigger signal obtained from scintillators. To account for this delay, the signal from the RPC is delayed such that it is shifted after the trigger is obtained using parameters like gate offset in the CAEN DPP software compatible with V1730. Thus, V1730 is an appropriate choice in these experiments.

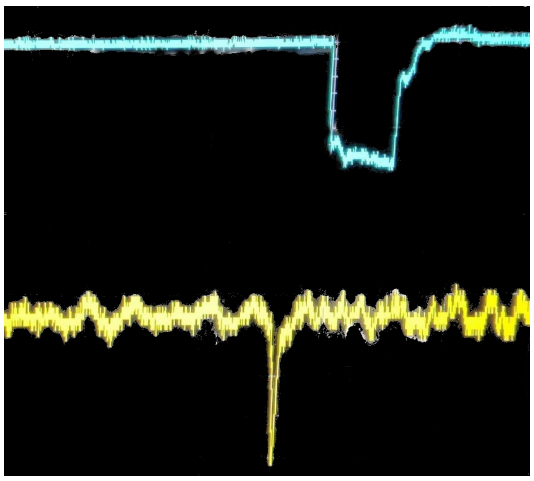

Figure 4.1: The signal is represented by the yellow waveform and the trigger is represented by the blue waveform.

Chapter 5

Simulation of RPC: Garfield++

Garfield++ is an object oriented toolkit used for simulation of gaseous detectors and semiconductor-based detectors. It is an advanced version of Garfield and is maintained by CERN. It was last updated in 2019 and the official guide is documented by Heinrich Schindler from CERN. It provides various interfaces that allows the use of external programs for different parts of the simulation process. The external programs used in this simulation are discussed in this chapter.

5.1 Components

The physics of the detection of muons has been discussed earlier. The same physical processes are implemented through this simulation. The first step is the construction of the detector which sets the dimensions and the composition of various components of the detector. The gas mixture used for the detection process is then defined, following by setting a track for the incoming particle, propagation of the electron avalanche with time and the resultant induction of signal on the readout strips. A flowchart describing the functionality of each package is shown in Fig. 5.1

5.1.1 ROOT Geometry Manager

For complex structures, the class `GeometryRoot` can be used which provides an interface to the ROOT geometry (`TGeo`). The structure of RPC detector is built using solid boxes (rectangular cuboids) stacked on each other. Overlaps are avoided

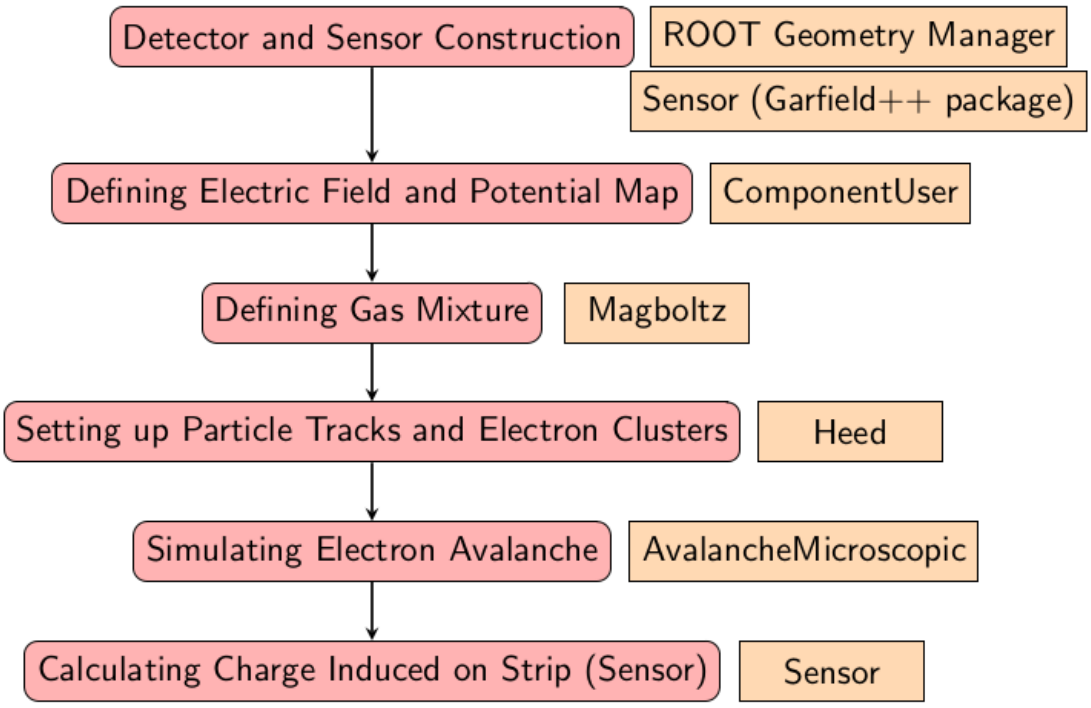

Figure 5.1: A flowchart showing the function of each package used in the simulation of single-gap RPC using Garfield++

and tested after the geometry is defined. The construction of the geometry has the following steps:

- The origin of the setup is taken to be the center of the gas-gap. The dimensions of every component are defined individually. For instance, the dimensions of the resistive glass plates are defined as follows:

  ```
  float xPlate = 30.0, yPlate = xPlate, dPlate = 0.2;
  ```

  Similarly, for other components, their extent in the three dimensions are defined.

- The materials for different components are defined using `TGeoMaterial`. For instance, the material copper is defined as an element with atomic mass, atomic number and density in g/cm^3.

  ```
  TGeoMaterial *mat_Cu = new TGeoMaterial("Cu", 63.55, 29,
  ```

```
8.96);
```

The Mylar sheets used in this experiment are hydrocarbon polymers, the chemical composition is $(C_{10}H_8O_4)_n$. For defining composite medium like Mylar sheets, the class `TGeoMixture` is used. Here, the number of constituents and the density of the material are defined. It is followed by defining each constituent and their relative mass in the composition.

```
TGeoMixture *mat_mylar = new TGeoMixture("Mylar",3,1.38);
mat_mylar->AddElement(12,6,120);
mat_mylar->AddElement(1,1,8);
mat_mylar->AddElement(16,8,64);
```

- The medium and the volumes are defined subsequently using the materials and the dimensions of the different components. For instance, the glass plates are defined as follows,

```
TGeoMedium *glass = new TGeoMedium("Glass", 3, mat_glass);
TGeoVolume *vol_plate = geom->MakeBox("Vol_plate", glass,
xPlate/2, yPlate/2, dPlate/2);
```

- The world volume is defined and the other components are added to `top` volume as nodes with their specific positions and dimensions. Finally, the geometry is closed and the construction is complete.

```
top->AddNode(vol_plate, 1, new TGeoTranslation(x0, y0,
(z0+dGas+dPlate)/2), "plate_top");
```

Using the ROOT Geometry, the detector geometry is plotted in a 2D canvas. It is shown in Fig. 5.2. It is a top view of the RPC along with the readout strips. The external electronics and the grounded plates are not shown in this figure.

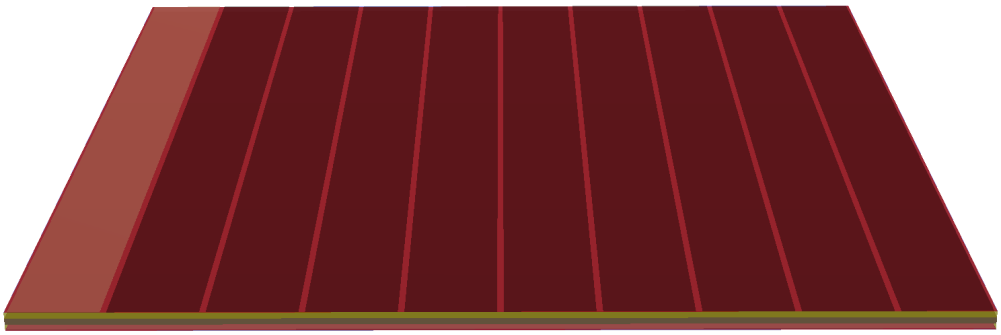

Figure 5.2: The detector setup as visualized by the ROOT geometry.

5.1.2 Magboltz

The gas mixture used in this experiment contains a Freon, Iso-butane and Sulphur Fluoride. The gas table is generated for a given gas composition using Magboltz. The class MediumMagboltz can be used for the calculation of transport parameters. It also provides access to the electron-molecule scattering cross-sections used in Magboltz. Hence, microscopic tracking is made possible.

Magboltz, written by Steve Biagi, is a program for the calculation of electron transport properties in gas mixtures using semi-classical Monte Carlo simulation. It includes a database of electron-atom/molecule cross-sections for a large number of detection gases.[3]

As input parameters, the temperature and pressure of the gas are specified, along with the gas composition. Following that, in this simulation, the maximum energy of the electron is also specified. It prepares a table of transport parameters (drift

velocity, diffusion coefficients, Townsend coefficient, and attachment coefficient) as a function of the electric field E (and, in general, also the magnetic field B as well as the angle between E and B).

5.1.3 ComponentUser

The electric field and potential in the active region and the surroundings is user-defined. Given the potential applied on the two surfaces of the glass electrodes, the field is calculated using ideal approximation of field distribution of a capacitor.

The electric field and potential maps generated for this experiment are shown in Fig. 5.3 and Fig. 5.4.

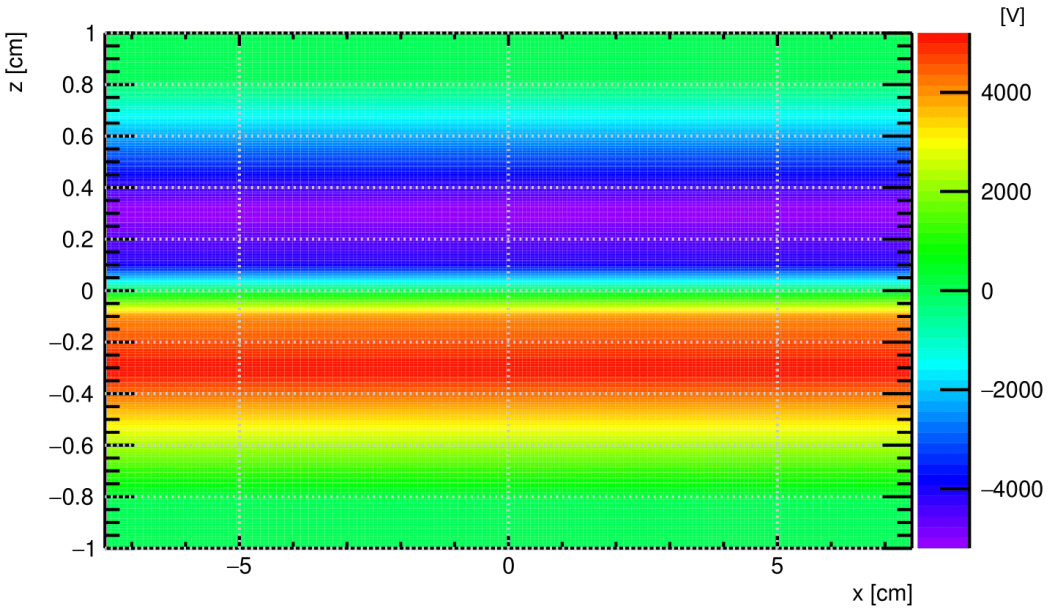

Figure 5.3: The electric potential map shown along the zx plane. The potential does not change along the xy plane. The applied potential difference is 10 kV.

The strip weighting field is calculated using an analytic expression for the field between two infinite parallel plates which are kept at ground potential except for the strip segment, which is raised to 1 V [3]. Using this definition and using the field

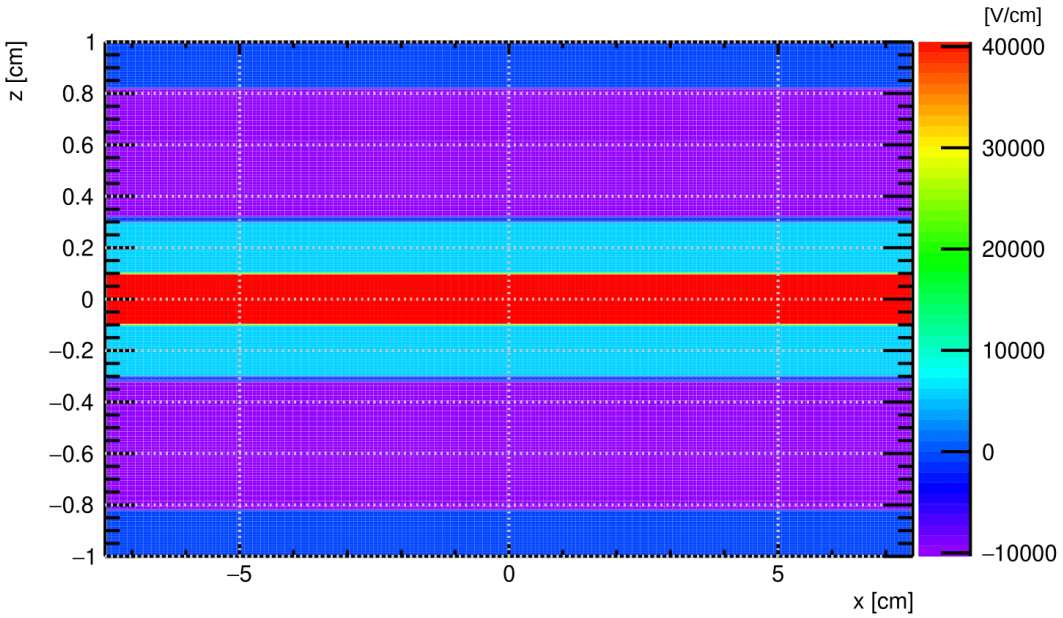

Figure 5.4: The electric field (E_z) map shown along the zx plane for the given potential distribution.

configuration in the current setup and dielectric constant ϵ_r of the plates and taking $V_W = 1$, the weighting field is:

$$E_W = \frac{\epsilon_r}{0.2 \times (2 + \epsilon_r)} \text{ cm}^{-1}$$

For the region except the gas-gap, this value is set to 0. Also, this field is only defined along the z-axis and the other components are set to 0. The details of the calculation are provided in the appendix.

5.1.4 Heed

In order to simulate the process of detection, a muon having 2 GeV energy is made to pass through the detector setup. The class `Track` in Garfield allows us to simulate the ionization pattern due to a charged particle passing through the defined medium. The track of the muon within the detector is set up using `TrackHeed`.

- An incident particle is initialized using `void SetParticle(mu-);` which is

a μ^- in this simulation.

- This is followed by setting an energy of the particle, a predefined `sensor` and enabling the electric field.

- A new track is initialized using the following
  `void NewTrack(const double x0, const double y0, const double z0, const double t0, const double dx0, const double dy0, const double dz0);`
  The first four are initial position of the track and the last three are the initial momentum of the particle.

- After successful initialization, the "clusters" produced along the track can be retrieved by
  `bool GetCluster(double& xcls, double& ycls, double& zcls, double& tlcs, int& n, double& e, double& extra);`

As a result, the information about the cluster of electrons formed due to the muon passing through the gas mixture is obtained. This information is the input required for generating the electron avalanche. The program Heed [I. B. Smirnov] is an implementation of the photo-absorption ionization (PAI) model. The `GetCluster` is called to obtain information about the electrons in the cluster.
`bool GetElectron(const unsigned int i, double& x, double& y, double& z, double& t, double& e, double& dx, double& dy, double& dz);`
In this simulation, the photon collision rates are not calculated, since the iso-butane in the mixture serves as a good absorber of ultra-violet photons.

5.1.5 Avalanche

The microscopic tracking involves following a particle from collision to collision. In Garfield++, the class `AvalancheMicroscopic` is used for microscopic tracking. As input, it requires a table of the collision rates for each scattering process as function of the electron energy. The calculations previously done by `MediumMagboltz` is used in this step of the simulation. The electrons are propagated in the defined field configurations in between collisions. The duration Δt of a free-flight step is sampled using the "null-collision" method. As higher energy is approached, the null-collision is also increased accordingly. The scattering process is sampled based on the relative collision rates at the new energy, the energy and direction of the electron are updated according to the type of collision afterwards. The class is used as follows

```
void AvalancheElectron(const double x0, const double y0, const
double z0, const double t0, const double e0, const double dx0
= 0., const double dy0 = 0., const double dz0 = 0.);
```

5.1.6 Sensor

As mentioned before in detection mechanism, the signal is calculated using the Shockley-Ramo theorem, represented by the equation 2.1. The steps to signal calculation are as follows:

- Calculating the weighting field for the sensor as done previously.
- The electrode to be used for signal calculation needs to be initialized as follows:

  `void sensor->AddElectrode(comp, "strip_x4");`

  Here `comp` is the pointer required to specify the weighting field.
- The binning for signal calculation is then specified.

```
void Sensor::SetTimeWindow(const double tmin, const double
tstep, const int nbins);
```

For this simulation, the value is set at 0 to 40 ns, with a bin width of 1 ns. The significant art of the signal lies between a few ns to 30 ns.

- The signal calculation is then enabled using the following:

```
AvalancheMicroscopic* aval = new AvalancheMicroscopic();
aval->EnableSignalCalculation();
aval->SetTimeWindow(tMin,tMax);
aval->EnableDriftLines();
```

- The signal is obtained at the i^{th} bin using the following:

```
current[i] = sensor->GetElectronSignal("strip_x4",i)*1000;
```

Here, a factor of 1000 is multiplied to obtain the current in nA.

- This current is added for each time bin to obtain the total charge induced.

```
Qstrip1 += fabs(sensor->GetElectronSignal("strip_x4",i))*tStep;
```

5.2 Signal

A sample signal obtained using the code is shown here in Fig. 5.5. This signal is obtained for 1% SF_6 in the gas mixture hen the potential applied across the electrodes is 11.0 V. The integrated charge of this signal is 0.0574633 pC, which is above the minimum threshold value of 0.025 pC used in the experiment. Also, the signal shape closely represents signals obtained from the experimental setup. The signal shown here is induced due to the motion of the electron avalanche inside the gas-gap. In the experiment, a signal due to the motion of ions inside the gap is also induced in the read-out strips but the current induced is order of magnitude lesser than the electron

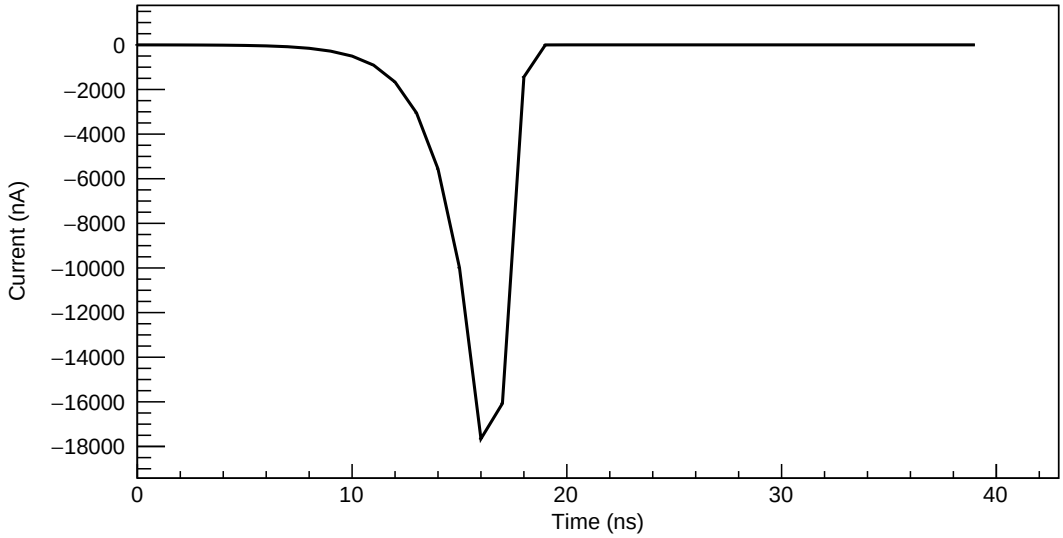

Figure 5.5: Sample signal from simulation

signal. Hence, the actual signal can be safely assumed to be the electron signal.

5.3 Analysis

The simulation has been run for the gas mixture containing 94.5% Freon, 4.5% isobutane and 1% SF_6. For potentials below 11.0 kV, the number of signals with charge above 0.025 pC are negligible. hence, the final simulation has been carried out for potential drops above 11.0 kV. Due to reasons discussed in the following section, the efficiency curve obtained from simulation differs from the curve obtained experimentally. For potential drop of 11.6 kV or higher, the signals could not be generated using our computational resources. Compared to the efficiency values obtained from experiment, the efficiency above the thresholds are low, which is a major drawback of Garfiled++ simulation. The simulation is still ongoing.

5.4 Drawbacks

Garfield++ is an effective tool for simulation of gaseous detectors, yet there are a few downsides of using Garfield++ for this simulation. The first major problem is how it deals with the creation and propagation of electron avalanche. Another problem arises due to the generation of single electron avalanche corresponding to ionization due to an incident charged particle.

- Garfield++ uses the `Magboltz` code to calculate the values of drift velocity, Townsend coefficient and attachment coefficient using a Monte Carlo method. In this simulation, microscopic tracking is used for the propagation of the electron avalanche. Both of these processes are computationally expensive, and hence time consuming. As the applied electric field increases, the time taken to generate events also increases to the point that suitable number of events can not be generated beyond a certain value of electric field.

- The simulation treats every event separately, also, for each tract generated by `TrackHeed`, one avalanche is generated, which might not be the case for the experimental case. This can be verified from the simulation itself as every particle track corresponds to one avalanche. This is not necessarily the case for experiment because the incident particle can undergo multiple collision with negligible loss in energy, thereby generating more than one ionizing electrons. Thus, the charge induced in an event in the experiment is usually higher than calculated from the experiment. This also explains the reduced efficiency above thresholds in the simulation.

Chapter 6

Construction of Double-gap RPC

From the experimental results of the single-gap RPC constructed using low-resistive glass plates, the estimated rate capability is around 3 kHz/cm^2, as mentioned in section 7.3. To achieve higher rate capability, the double gap design of RPC is implemented. In this design, the space localization is compromised along one axis. Thus, either the x or y coordinate of the incident particle can be determined using one double-gap setup. One can modify this design by adding more read-out strips to obtain localization in the other other coordinate. The setup prepared is the simplest version of the double-gap configuration and the design is as follows.

- Two RPCs are constructed similar to the single-gap setup.
- A collection of read-out strips parallel to the x-axis is prepared on plastic.
- The read-out strips are placed between the RPCs, insulated using two Mylar sheets.
- The surfaces facing the read-out strips are grounded and the other two surfaces are connected to high voltage.

6.1 Detection Mechanism

The design is expected to increase the efficiency at high particle flux. Detectors like RPC, when exposed to high luminosity, lose their optimum efficiency. The rate

capability can be estimated from the mean charge generated inside the gas-gap using the relation

$$\text{Rate Capability} = \frac{V}{\rho\langle Q\rangle t}$$

Here $\langle Q\rangle$ is the mean charge inside the gas-gap. When $\langle Q\rangle$ is larger the rate capability decreases. No source of muons with high flux was available, hence, the efficiency vs flux could not be plotted. This plot has been taken from the Journal of Instrumentation, High rate, fast timing Glass RPC for the high η CMS muon detectors.

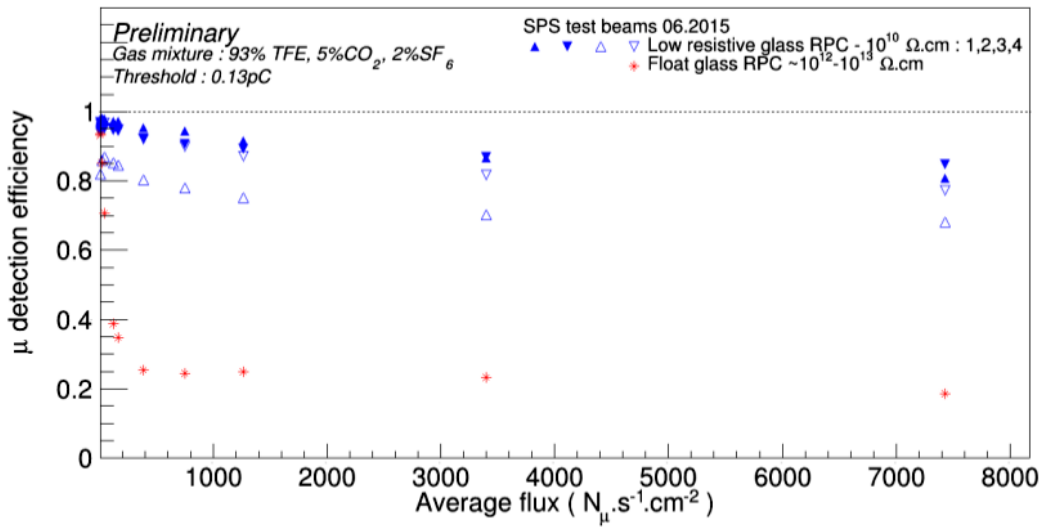

Figure 6.1: Efficiency of the five detectors with a pad readout as a function of the mean particle flux in SPS. [4]

It is evident that the efficiency decreases with increasing flux. Thus, in high flux, the efficiency needs to be enhanced. This can be achieved with the double-gap setup. Here, we have two different chambers stacked with a readout in between. Then potential is so applied that the electron-avalanche generated always moves away from the strips. This is shown in the following Fig. 6.2.

Thus, the total charge induced on the strip is almost twice the induced charge for single gap setup. Hence, for a given incident particle, for which the induced charge

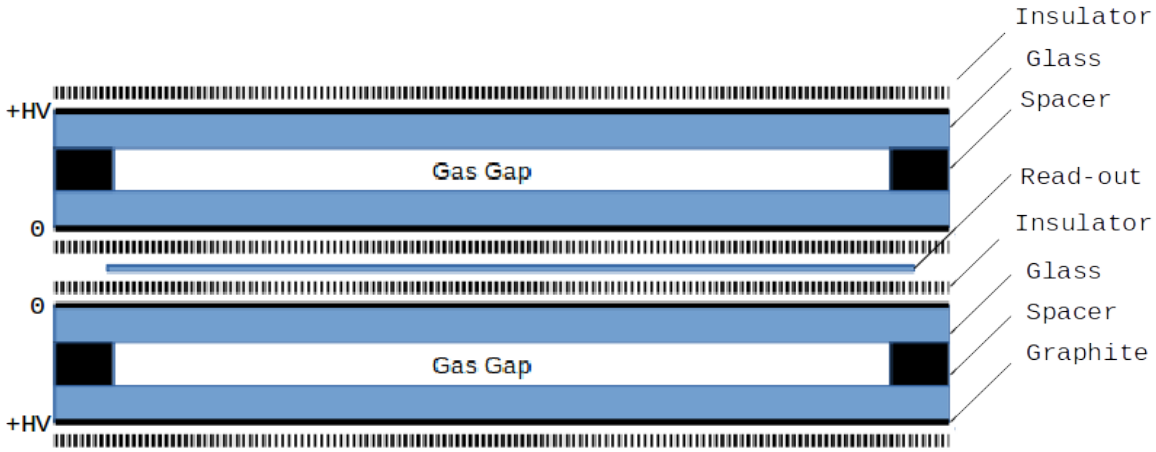

Figure 6.2: Schematic diagram of double-gap RPC cross-section

was below the cut-off charge, will now lead to induced charge above the cut-off.

6.2 Construction

The construction process is similar to that of the single-gap RPC, except the specialized read-out strips and that two chambers are required. The construction of RPC chambers has been discussed in chapter 3. In this particular setup, the surface resistivity is kept at roughly 1 MΩ/□. The read-out strips had a conductor plate that was previously grounded, in this setup, that plate is removed.

Due to unavailability of another pair of low- resistive glass plates, these chambers are constructed of regular silicate glass. Also, the spacers used for construction of the chambers are different and perform better on the leak-test without the need of excessive glue.

6.3 Assembly

The setup cross-section is shown in the previous section. The assembly is done accordingly following the order in which the components are placed.

- The trigger setup is same as that for single-gap RPC. Here also, we have three plastic scintillator detectors, two below the setup and one above.
- Mylar sheets are placed above and below the setup to insulate the plates and also protect the graphite paint on them.
- The two chambers are placed inside these Mylar sheets.
- A read-out panel containing only copper strips is placed in between the two chambers.
- The graphite surfaces facing the read-out strips are grounded using a copper strip attached to the graphite paint.
- The surfaces away from the strips are connected similarly to high-voltage source.
- A different with opposite applied potential is also tried. In this case, the induced charge will have opposite sign.
- The gas is supplied using one single channel passing through one chamber and its outlet is connected to the inlet of the other chamber. This reduces the amount of gas used in the experiment.

6.4 Outlook

This setup is yet to be tested. Till now, by passing the gas mixture containing 95% Freon, 4.5% Iso-butane and 0.5% SF_6, the base current obtained was within 5 mA, which is sensible for the experiment. The ambient conditions are yet to be optimized. The testing of this detector setup remains unfinished.

Chapter 7

Summary and Conclusions

The experiments done throughout the project are aimed at characterizing the detector. It includes calculating the noise rate, efficiency at different configurations, estimating the rate capability of the detector and the strip multiplicity. While the later is aimed at localization of the signal, the relevant properties for estimating the rate capability are the mean charge deposited inside the gas gap and the range of potential difference over which the efficiency is almost constant.

7.1 Efficiency

The efficiency at different thresholds of deposited charge is the ratio of the number of events with charge deposition above the threshold value to the total number of events. The efficiency curves have been obtained for four different threshold values of 25 fC, 50 fC, 100 fC and 200 fC.

The points for each threshold for each gas mixture are fitted with the following **sigmoid function**:

$$y = \frac{A}{1 + \exp\left[B(x - C)\right]} \tag{7.1}$$

Here, A is the maximum efficiency achievable by the detector, B gives the slope or rate at which the efficiency increases with potential and C gives the potential at which efficiency is half of the maximum. In general, the maximum efficiency is close to 1, hence C gives the potential at which the efficiency is 1/2.

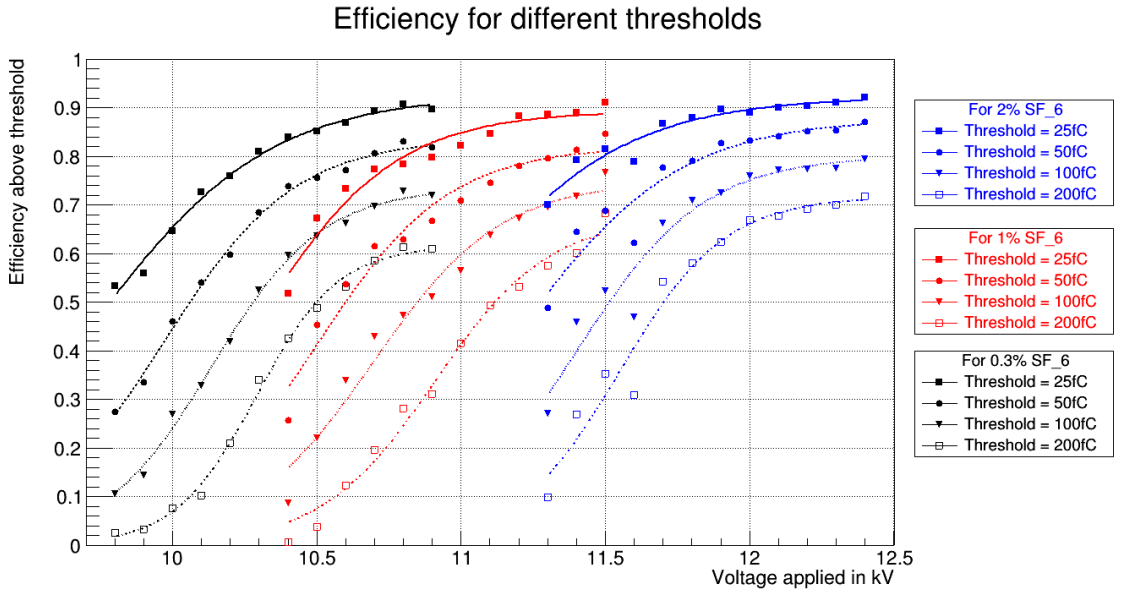

Figure 7.1: Efficiency of the RPC detector for different gas mixtures as a function of applied potential difference.

The efficiencies increase with applied potential difference monotonically and reduce as the threshold charge is increased. The efficiency curves also provide the tolerance level of the detector operating with different gas mixtures. From the plot, it can be inferred that the efficiency is constant for 200 V from 10.7 kV to 10.9 kV with 0.3% SF_6 in the mixture. The efficiency is constant for 1% SF_6 in the mixture for about 300 V and for 2% SF_6 in the mixture, it is around 500 V. For calculation of rate capability, the range is taken to be 300 V.

7.2 Mean Charge

The mean charge per event deposited on the strip for different gas mixtures and different thresholds of deposited charges are shown below. Here, as we expect, the mean charge is increasing with increase in threshold and also with increase in potential as higher potential difference implies greater cluster size of electrons forming inside the gas gap.

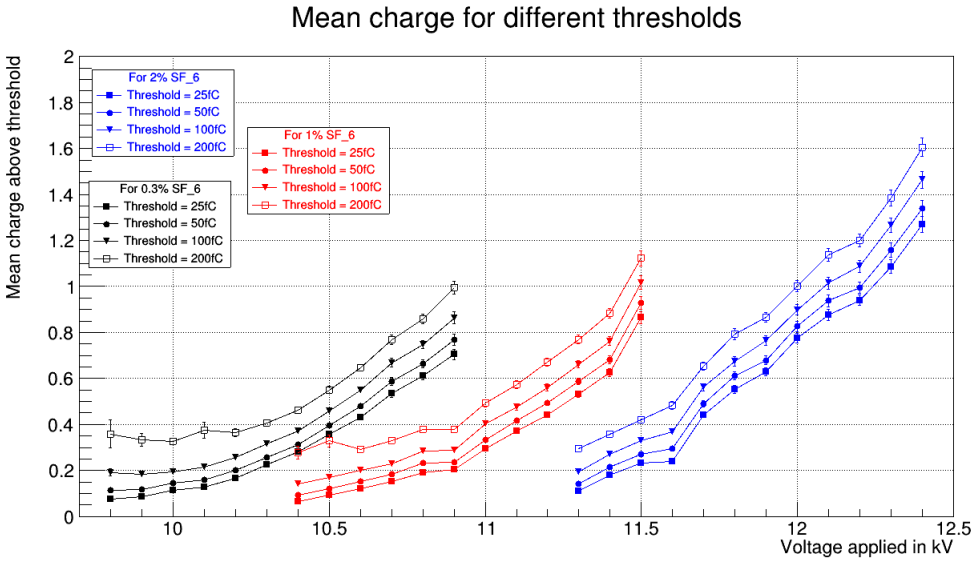

Figure 7.2: The mean charge of the signals obtained for different gas mixtures as a function of applied potential difference.

7.3 Rate capability

The rate capability can be estimated from the efficiency and mean charge data obtained from experiments. The following table gives the estimates for different gas mixtures and operating potentials. The estimation for 0.3% SF_6 in mixture is given by:

$$\Gamma = \frac{V}{\rho \langle Q \rangle t} = \frac{200}{(1.5 \times 10^{10}) \times (25 \times 0.637 \times 10^{-12}) \times 0.4} \text{ Hz/cm}^2$$

Here, the factor of 25 is the ratio Q/q, where Q is the charge deposited inside the gas gap, ionic charge, and q is the prompt induced charge in the readout strip [2]. For

SF_6 in mixture	Mean charge	Rate capability (kHz/cm^2)
0.3%	0.637	3.14
1.0%	0.652	3.07
2.0%	0.646	3.10

Table 7.1: Estimated rate capability with threshold 100 fC with almost 70% efficiency

different efficiencies, the mean charge deposited is different and hence, we can obtain a

rate-capability vs efficiency curve. The following Fig. 7.3 compares the rate-capability vs efficiency curve for different gas mixtures within a given window of efficiency. It

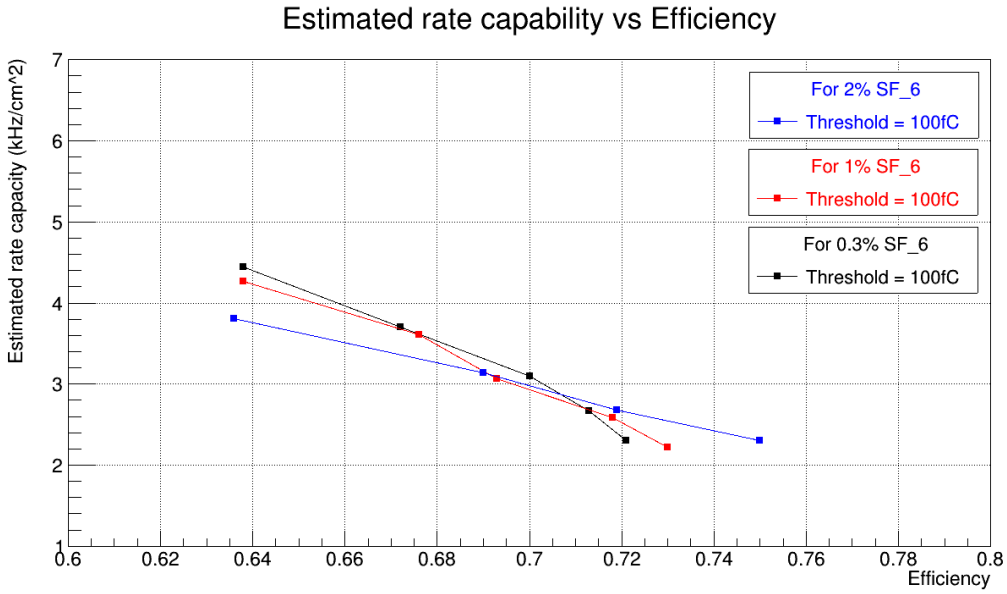

Figure 7.3: Estimated rate capacity vs efficiency of cosmic muon detection using the RPC detector, the points with efficiencies between 0.6 and 0.8 are shown.

can be seen that curves show an expected decreasing nature, which implies that high rate capability is achieved at the cost of efficiency. Also, for higher values of efficiency, the gas mixture with 2% SF_6 is a better choice.

7.4 Strip Multiplicity

In an ideal case, if a radiation is incident on a certain position of the detector, only the strip above and below should show signals. This is not so in reality. The charge gets induced in multiple strips. Thus we have to look at the multiplicity or cluster size of the detector and keep it as minimum as possible. It is preferable to have an average cluster size of around 2. The cluster size for different threshold values of charge deposited for 0.3% SF_6 gas mixture are shown in Fig. 7.4. The cluster size reduces with increase in threshold. The cluster size is also slowly increasing with

voltage.

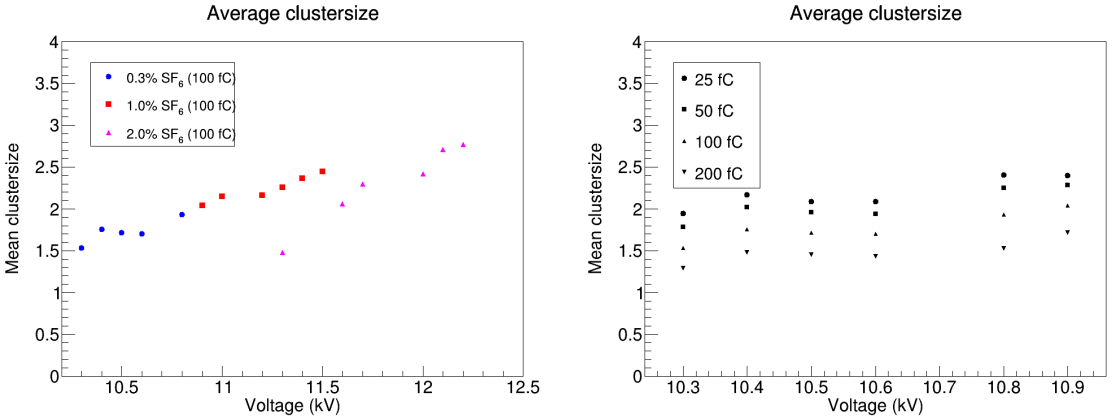

(a) (b)

Figure 7.4: Plots showing the strip multiplicity for different gas mixtures with 100 fC threshold (a) and the strip multiplicity for different thresholds using 0.3% SF_6 in the mixture (b).

7.5 Efficiency of strips

By looking at the detection efficiency of the readout strip just below the trigger scintillator and strips farther away from it, we get an estimate of the cluster size. The strip just below the trigger scintillator has maximum efficiency in most cases as expected. The efficiency of the other two strips is comparable to the one just below the paddle because of oblique incidence of muons or incidence in between strips.

7.6 Noise Rate

The first set of experiments were carried out by connecting a single strip from the RPC to the digitizer and looking at the noise rate. **Noise rate** is given by the number of signals obtained in a second on an unit of area. The noise rate for different gas mixtures at different potential differences across the electrodes.

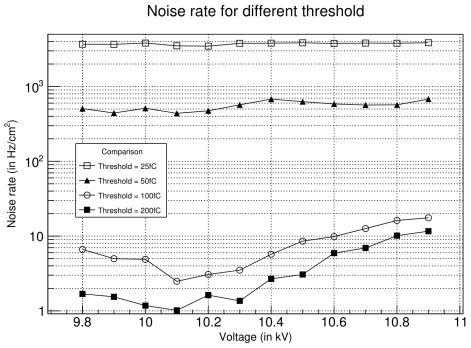

(a) Noise rate for 0.3% SF_6 in the gas mixture.

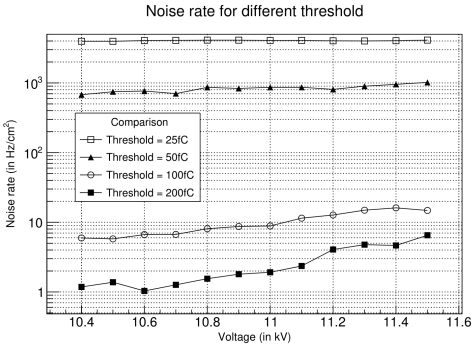

(b) Noise rate for 1.0% SF_6 in the gas mixture.

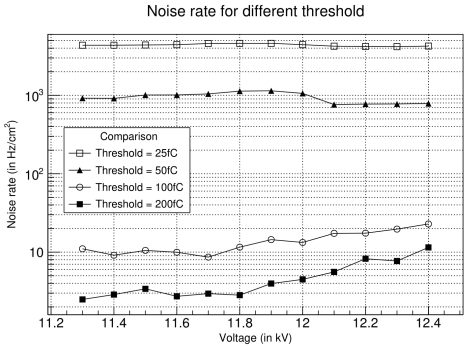

(c) Noise rate for 2.0% SF_6 in the gas mixture.

Figure 7.5: Noise rate plots for various gas mixture compositions.

7.7 Inference from Simulation

From the simulation, the efficiency of muon detection vs the applied potential curve is obtained. Since, the simulation is incomplete, this result can not be compared quantitatively with the experimental result. Yet, it shows the same increasing nature as the experimental result. It also shows the efficiency of detection at a given applied potential obtained from simulation is lesser than the one obtained from experiments. Similar observations has been reported in another simulation method that uses Garfield++ to generate initial conditions.[5] The efficiency vs applied potential curve for the gas mixture containing 1% SF_6 in the mixture is shown in Fig. 7.6. The points obtained have very low statistics. We are aiming to use an alternate code to obtain around 2000 events, which is comparable to the number of events obtained for each potential from the experiment. We could not generate significant number of

events for applied potential over 11.4 kV.

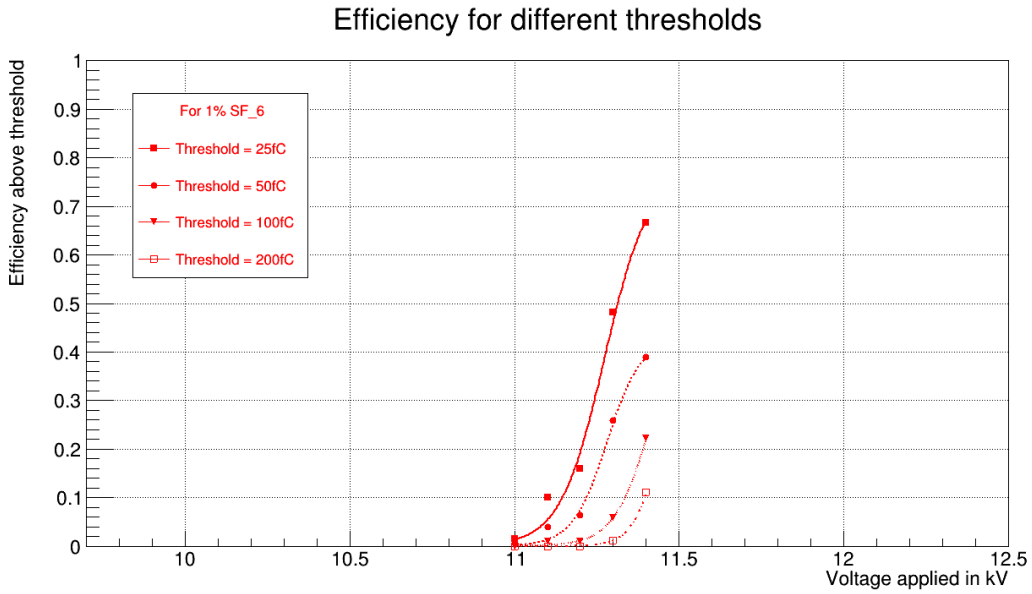

Figure 7.6: Efficiency of the RPC detector for different gas mixtures as a function of applied potential difference as obtained from simulation using Garfield++.

7.8 Conclusion

Through the experiments, we predict that the single gap RPC detector made of low resistive glass plates with 2 mm gas gap has a rate capacity of at least 3 kHz/cm^2 using Freon(R134a) as the gaseous medium, with iso-butane and slight amount of SF_6. This rate capability is estimated by setting the threshold of induced charge at 100 fC, for which the noise rate is of the order of 10 cm^{-2}·s^{-1}.

7.9 Outlook

The expected rate capability of 10 kHz/cm^2 is yet to be achieved. Also, the method of the simulation needs to be modified for higher electric field. The following are some possible ways to improve the performance of the detectors and the simulation.

- The double-gap setup remains to be tested.
- Reducing the gas-gap might help reduce the charge deposited in the gas gap and finally increasing the rate capability.
- An alternate code is yet to be prepared that can simulate the avalanche formation at high electric fields.
- The noise-rate can be reduced by methods like putting the setup in a dust free environment within a Faraday cage.

References

[1] Private communication with developers of low resistivity glass, Tsinghua University group, China.

[2] G. Aielli et al 2016 JINST 11 P07014, Improving the RPC rate capability.

[3] H. Schindler, Garfield++ User Guide (Version 2019.4)
`http://garfieldpp.web.cern.ch/garfieldpp/`

[4] F. Lagarde et al 2016 JINST 11 C09006, High rate, fast timing Glass RPC for the high η CMS muon detectors.

[5] Frederic Van Assche, thesis, Universitiet Gent, Development of a Resistive Plate Chamber detector simulation framework.

[6] Fabio Sauli, Gaseous Radiation Detectors: Fundamentals and Applications (Cambridge University Press, 2014).

[7] R. R. Shinde, E. Yuvaraj, Fabrication and Characterization of Glass Resistive Plate Chamber (RPC), TIFR.

Appendix A

Electric field and Potential Map

The electric field and potential is defined manually for the simulation. Basic electrostatics is used for this purpose along with assuming the setup to be a capacitor. This assumption is valid since the detection of signal does not change applied potential by any significant value. Hence, the electric field inside the gas gap, `Ez` takes the following form:

$$Ez = 2.0 \times \frac{V_0}{((1.0 + (2.0/\epsilon_r)) \times 0.2)}$$

where V_0 is the absolute value of the potential applied to each plate. Subsequently, using $-\vec{E} \cdot d\vec{r} = V$, the electric field of all regions are calculated. The gas gap is assumed to have the same dielectric constant as air, the dielectric constant of the plates is 9.0.[1] The dielectric constant of the Mylar sheets is 0.5032 and that for the gap between the readout strips and the grounding plates is 1, since hollow plastic is used to separate them. The perpendicular component of the electric displacement vector is constant across the surface with no net free charge.

The part of the code used to define the electric field and potential is attached here.

```
float V0 = 5600, rel_per = 9.0,
value_Ez = 2.0*(V0/((1.0+(2.0/rel_per))*0.2));
void Field_map(const double x, const double y, const double z,
```

```
double& ex, double& ey, double& ez)
{
if(x<15.0 && x>-15.0 && y<15.0 && y>-15.0)
{
if(z<=0.1 && z>=-0.1)
{
ex=5., ey=5., ez=value_Ez;
}
   else if(abs(z)>0.1 && abs(z)<=0.3)
{
ex=0.0, ey=0.0, ez=(V0-(value_Ez*0.1))/0.2;
}
   else if(abs(z)>0.3 && abs(z)<=0.3100)
{
ex=0.0, ey=0.0, ez=-V0/(0.5032*3.1);
}
   else if(abs(z)>0.3100 && abs(z)<=0.3200)
{
ex=0.0, ey=0.0, ez=0.0;
}
else if(abs(z)>0.3200 && abs(z)<=0.8200)
{
ex=0.0, ey=0.0, ez=-V0/0.5032;
}
}
else
```

```
{
ex=0.1, ey=0.1, ez=8000;
}
   if (z>0.82 || z<-0.82)
{
ez=0.;
}
}

   void Potential_map(const double x, const double y, const dou-
ble z, double& V)
{
if(x<15.0 && x>-15.0 && y<15.0 && y>-15.0)
{
if(z<=0.1 && z>=-0.1)
{
V=-z*value_Ez;
}
   else if(abs(z)>0.1 && abs(z)<=0.3)
{
V=-((z-0.1*(abs(z)/z))*(V0-(value_Ez*0.1))/0.2+
(value_Ez*0.1*(abs(z)/z)));
}
   else if(abs(z)>0.3 && abs(z)<=0.3100)
{ V=-(-(z-0.3*(abs(z)/z))*V0/(0.5032*3.1)+(V0*(abs(z)/z)));
}
```

```
   else if(abs(z)>0.3100 && abs(z)<=0.3200)
{ V=-(-(0.01)*V0/(0.5032*3.1)+V0)*(abs(z)/z);
}
   else if(abs(z)>0.3200 && abs(z)<=0.8200)
{
V=-(-(z-0.3200*(abs(z)/z))*V0/(0.5032)+
(-(0.01)*V0/(0.5032*3.1)+V0)*(abs(z)/z));
}
}
else
{
V=z*5;
}
   if (z>0.82 || z<-0.82)
{
V=0.0;
}
}

   void WtField_map(const double x, const double y, const dou-
ble z, double& wx, double& wy, double& wz, const string strip)
{
if(z<=0.1 && z>=-0.1)
{
if(x<15.0 && x>-15.0 && y<15.0 && y>-15.0)
{
```

```
wx=0.1, wy=0.1, wz=rel_per/(0.2*(2+rel_per)); // Weighting field
values in V/cm
}
else
{
wx=0.0, wy=0.0, wz=0.0; // Weighting field values in V/cm
}
}
else
{
wx=0.0, wy=0.0, wz=0.0;
}
}
```